A Software-defined Underwater Acoustic Networking Platform for Underwater Vehicles

Deniz Unal, Sara Falleni, Emrecan Demirors, Kerem Enhos, Stefano Basagni, Tommaso Melodia
Institute for The Wireless Internet of Things, Northeastern University, Boston, MA, USA
E-mail: {unal.d, falleni.s, e.demirors, enhos.k, s.basagni, melodia}@northeastern.edu

ICC 2022 - IEEE International Conference on Communications | 978-1-5386-8347-7/22/$31.00 ©2022 IEEE | DOI: 10.1109/ICC45855.2022.9839033

***Abstract*—Underwater vehicles (UVs) are becoming essential for a vast range of novel commercial, scientific and military applications. These include seabed exploration, monitoring of critical infrastructure and resources, and coastal surveillance. However, usage of UVs is currently beset by limitations preventing them to carry critical equipment, such as agile wireless communication systems, which would facilitate and enable those applications. To overcome these limitations, in this paper we present the design blueprint and evaluation of a *wireless UV*, obtained by integrating a custom software-defined underwater acoustic networking platform integrated to a UV. We first describe the integration of the platform with a commercially available UV. We then present results from experimental campaigns at sea using our wireless UV to generate datasets for studying the Doppler effect due to mobility. Our results indicate the effectiveness of our design for ease of deployment and dataset generation.**

I. Introduction

Underwater vehicles (UVs), whether manned such as Remotely Operated Vehicles (ROVs) or Autonomous (AUVs), are the ideal mobile platforms for a vast range of novel commercial, scientific and military applications. UVs can be used at offshore oil and gas fields for high-quality video streaming to an operator via a tether cable. In this kind of scenarios a UV could use mechanical arms to perform inspection, maintenance and repair of underwater structures [1], [2], [3]. UVs can also be deployed to perform seabed exploration and marine research [4], [5], and for continuous tactical surveillance [6].

Despite the host of applications where UVs play a key role, their usage is limited as they are rarely designed to carry agile wireless communication systems that provide the data rate needed to support most applications and that adapt to swiftly varying underwater conditions. Most UVs depend on cables to maintain continuous connection with an operator to send and receive commands (i.e., remote guidance) and data (i.e., sensor readings, videos) [7]. Nevertheless, such tethered ROVs are inherently limited in terms of speeds, maneuverability and range due to their tether cables [8]. Furthermore, deploying tethered UVs in large areas can be prohibitive in terms of cost and time, as they require long and expensive tether management systems as well as a vessel capable of handling these systems for the entire duration of their deployment [9].

Untethered UVs such as AUVs can overcome most of the limitations introduced by tethering. They can also operate without requiring a deployment vessel for long periods of time (i.e., up to several days) [9]. However, AUVs can only offer limited control and feedback during operations. Their mission is predefined and it can only be changed when the vehicle is on the surface and has some sort of connection with a pilot or control station. While there have been some commercial solutions to address these limitations and to offer real-time control and data transmission capabilities for AUVs [10], data rates are still abysmal (tens of bps) and transmission ranges often very short (< 200 m). Moreover, their modem design does not allow them to adequately adapt to the rapid space and time-varying underwater channel and interference conditions.

To address these limitations, in this paper we describe and evaluate the integration of a custom software-defined underwater acoustic networking platform, the SEANet modem [11], to a commercially available UV. Our integration will *provide the UVs with the capability of establishing high data rate, robust, self-optimizing wireless acoustic links in spatially and temporally varying environments*. Our *wireless UV* will be able to obtain real-time control and data communications wirelessly, as well as operate in networks of self-configuring, mobile and wirelessly connected devices. The software architecture for data transfer between mobile underwater nodes can also be extended to build a swarm of underwater drones.

The main contributions of this article are as follows:

- **Design blueprint**. We provide the design blueprint of a wireless UV. Particularly, we describe the software, hardware, and mechanical design that can be used as a guide for developing future wireless UV platforms. Our design is showcased by the prototype from integrating the SEANet software-defined underwater acoustic modem with the Blue Robotics BlueROV2 (Fig. 1).[1]

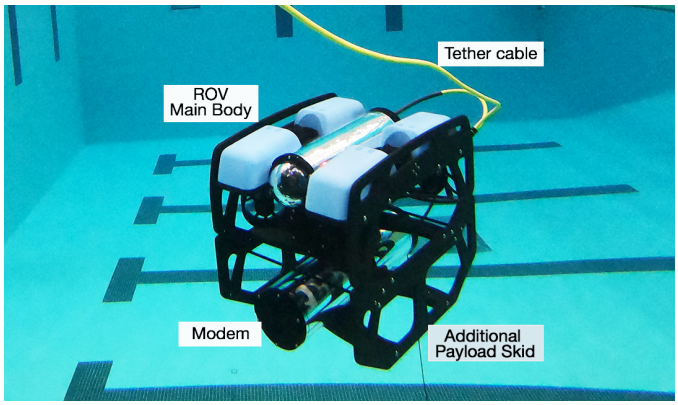

Fig. 1: Integrated SEANet software-defined underwater acoustic modem and Blue Robotics BlueROV2.

[1] To ease control and repeatability of experiments we use a COTS tethered device. The tether is only used for controlling the movement of the ROV.

- **Dataset generation and evaluation**. One of the greatest challenges of underwater acoustic communication is the severe Doppler distortion due to mobility [12]. The effect is significant even for relatively slow speeds and it limits the link performance of mobile nodes. In order to achieve high data rates in mobile scenarios, the effect of Doppler shifts needs to be compensated at the receiver. Existing research works on Doppler correction algorithms often rely on prerecorded datasets for performance evaluation since data collection is a challenging task. Our proposed integrated platform can alleviate this problem by enabling the generation of authentic real-world datasets for studying the Doppler effect. Here we report the results from a set of experiments at sea, where we use our integrated platform programmed with arbitrary trajectories and acceleration profiles to emulate mobility. A sample dataset is generated and link performances are characterized with different physical layer parameters under varying mobility and channel conditions.

The rest of the paper is organized as follows. Section II describes the integrated platform. Section III presents the sample dataset and results obtained with the integrated platform at sea. Finally, Section IV concludes the paper.

II. System Description

The system is realized with a COTS UV platform, namely the BlueROV2 by BlueRobotics. The platform was chosen because of its flexibility and open architecture both in terms of hardware and software. The software-defined, high data rate, underwater acoustic SEANet modem integrated into the BlueROV2 enables the system with high data rate acoustic communication capabilities [11].

Mechanical Design. A payload skid, compatible with the vehicle, and attached under the main body of the ROV, holds the modem. The payload skid has several mounting points that can be used for different purposes such as additional lights, weights, and additional enclosures. Using these mounting points, we were able to mount our high data rate modem on the ROV. The addition of the modem and the payload skid affects the kinematics of the ROV. The cylindrical modem enclosure adds buoyancy to the mobile node, lifting it over the waterline. Similarly, the weight of the modem and payload skid shifts the center of mass of the ROV. Increased net buoyancy leads to poor dive performance as some of the ROV thrusters are not fully submerged and are unable to displace water. This is countered by mounting a total of $400\,\mathrm{g}$ ballast weight blocks to the bottom side of the payload skid. Another issue observed was the presence of downward forces when moving forward. The modem enclosure was shifted and ballast weight positions were rearranged by trial and error to alleviate this unwanted movement. The modem is encapsulated in a 4-inch cylindrical acrylic pressured enclosure and insured to the skid using a pair of clamps.

Hardware Design. As it can be seen in Fig. 2, power is supplied to the SEANet modem through the battery enclosed on the ROV. Also, the main module is connected to the companion computer on the ROV for necessary data communication between the modem and the ROV through a standard Ethernet interface. The data cable, in particular, connects the standard Ethernet interface of the modem with the USB interface of the Companion Computer. The Companion is used as a bridge between the laptop on the ground and the modem, and the tether cable, kept in this early phase for safety and convenience purposes, provides connectivity for both the ROV and the modem to the ground station.

The hardware design of the SEANet modem is structured in five modules: power, main, converter, communication, and switch module. A transducer is directly attached to the switch module. Each module is implemented on a separate printed circuit board; the boards are interconnected with standard PCI Express connectors with a custom interface. The power module is implemented with a surge suppression circuit that continuously monitors the voltage and current levels of the battery, that supplies power to all the modules that are used in the modem. The main module in our case is a MicroZed development board based on the Xilinx Zynq-7000 SoC. It includes Programmable Logic (PL) that handles physical layer functionalities and Processing System (PS) that handles upper layers functionalities. PS and PL are connected with an advanced extensible interface (AXI) buses. The converter module includes an analog-to-digital converter (ADC) and a digital-to-analog converter (DAC) to interface the analog and digital domains. It includes LTC1740 as the ADC, operating on 14 bit parallel outputs up to $6\,\mathrm{Msample/s}$ sample rate, and LTC1668 for DAC, operating on 16bit parallel inputs up to $50\,\mathrm{Msample/s}$ sample rate. Two communication modules, a power amplifier, and a preamplifier are attached to transmit and receive chains. The power amplifier is based on APEX PA340 high voltage amplifier that is powered by a fly-back converter circuit in boost configuration. The module amplifies the 1 V_{pp} output of the DAC to 100 V_{pp} to be transmitted with the transducer. The preamplifier module interfaces with the received signal from the transducer and consists of multi-stage amplifiers and a filter. The signal is band-pass filtered between 10 kHz and 250 kHz in order to eliminate out-of-band noise that may be originated from an acoustic or electrical domain.

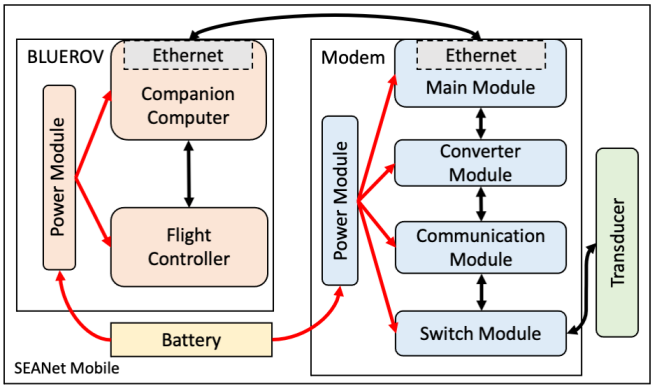

Fig. 2: System hardware design.

Finally, the filtered signal is amplified by an AD8330 variable gain amplifier (VGA) which can be controlled digitally from the main module. The total gain of the preamplifier module can be adjusted between 40-90 dB. The switch module includes the relevant connections between the modules and a reed relay to alternate transmission and reception operation. The transducer used is a B-Tech BT-H150 broadband unidirectional transducer, which can be used as a projector with a resonance frequency of 145 kHz. The transducer is mounted on a tapped hole on the end-cap of the modem enclosure. The vertical beam-pattern of this transducer is cardioid with $3\,\mathrm{dB}$ loss at 30° off its acoustic center. To that end, the modem is integrated to the ROV where the transducer unit facing forward to utilize the cardioid beam pattern efficiently. All the modules described above are custom-made but have standard interfaces that allow easy development and upgrade.

Software Design. The software design of the modem can be divided in terms of Processing System (PS) and Programmable Logic (PL). The PS runs a custom version of Linux 4.19 for embedded devices; it offers a standard Ethernet interface to the user that can then easily connect to it. More specifically a user can utilize standard UDP and TCP protocols to send data to or receive data from the modem using the IP address of the Ethernet interface. The communication between PS and PL, which are connected through AXI buses and DMAs, is handled by a Linux Kernel Driver. The main Programmable Logic design implements Zero Padded Orthogonal Frequency Division Multiplexing (ZP-OFDM) technique to send and receive packets in the form of binary data. BPSK, QPSK, and 16QAM modulation schemes are available in the system. Another implementation is the *"base"* PL for transmitting and receiving arbitrary waveforms in the format of raw data to be processed by software such as GNU Radio or MATLAB. The *"base"* PL consists of an upconverter, a downconverter, a direct digital synthesis, digital gain control blocks which can be configured from the PS. While ZP-OFDM PL has configuration capabilities for packet parameters such as the number of symbols and guard intervals, *"base"* PL offers more flexibility at the physical layer at the expense of processing power. These capabilities are crucial for adaptation to the current environment for best link performance. The modem can utilize bandwidths and center frequencies above $100\,\mathrm{kHz}$ which is significantly larger than the bandwidths that are used by commercial underwater acoustic modems like Teledyne Benthos ($5\,\mathrm{kHz}$) or Kongsberg Modems ($10\,\mathrm{kHz}$). On the other hand, system performance is capped by the frequency response of the transducer and amplifier boards in use.

III. Performance Evaluation

Using the platform, we have conducted preliminary experiments at sea. In these experiments, we demonstrated reconfigurable high-rate communication capabilities, and we recorded a dataset with Doppler shifts. The experiments were performed at a boat dock in the Charlestown neighborhood of Boston, Massachusetts. The dock is located between a marina and a wharf, and it is open to Boston Harbor. While open sea conditions are not observed, the area is exposed to marine traffic and mild currents. The location of the deployment affects the link geometry and therefore the underwater acoustic channel. It is important to note that surface reflections are a concern for experiments in constricted environments (e.g. swimming pools) and as a consequence, severe multipath may be observed. Using a Garmin Striker 4, we estimated the depth around the area to be 5.5 m, a value that matches with the nautical chart for the harbor.

In our setup, a modem integrated into a UV (mobile node) and a modem with a fixed location (static node) were used as shown in Fig. 3a. The static node stays on the shore with its transducer submerged off the side of the dock. The modems on both nodes have identical configurations except the static node, which is primarily used as a receiver node during the experiments, is equipped with a Teledyne Reson TC4013 transducer. As a reference hydrophone by design, TC4013 can offer a flat frequency response with an unidirectional beam pattern which is ideal for receiver operation. The experiments were controlled from a host computer that connects to both nodes. The mobile node uses the multiplexed connection described in Section II whereas the static node has an Ethernet connection to the host computer. Both of the modems were accessible through secure shell connections initiated from the host computer during the deployment.

For the PL implementation, *"base"* mode is preferred for these experiments since it enables custom waveform transmission and recording capabilities. On the transmit side, *"base"* PL mode allows us to make fine adjustments to the ZP-OFDM packet parameters at the dock. Similarly, data collection is possible on the receiver side with the same design. System parameters such as transmit gain level, receiver pre-amplifier gain, ADC and DAC sample rates, and center frequency are adjusted through the modem configuration software. ADC and DAC sample rates are set to $1.25\,\mathrm{Msample/s}$.

The packet structure used to perform the first set of experiments consists of a preamble, OFDM symbols, and a postamble sequence with guard intervals in between. The preamble and postamble are used for signal detection, synchronization, and Doppler estimation, whereas the OFDM symbol is used for estimating the bit error rate performance of the system. For preamble and postamble signals, maximum length sequences are used. Signal detection and synchronization are performed with the auto-correlation method. For the Doppler shifts estimation, the method described in [13] is used. We define T_{TX} as the packet duration measured from the preamble and postamble correlation points. The same duration is then estimated at the receiver as T_{RX}. Time compression or dilation due to mobility can be observed based on the deviation of T_{RX} from T_{TX}. Doppler scaling factor a quantifies the effect and is calculated as follows:

$$a = \frac{T_{RX}}{T_{TX}} - 1 \tag{1}$$

The relative speed between the mobile and static nodes can

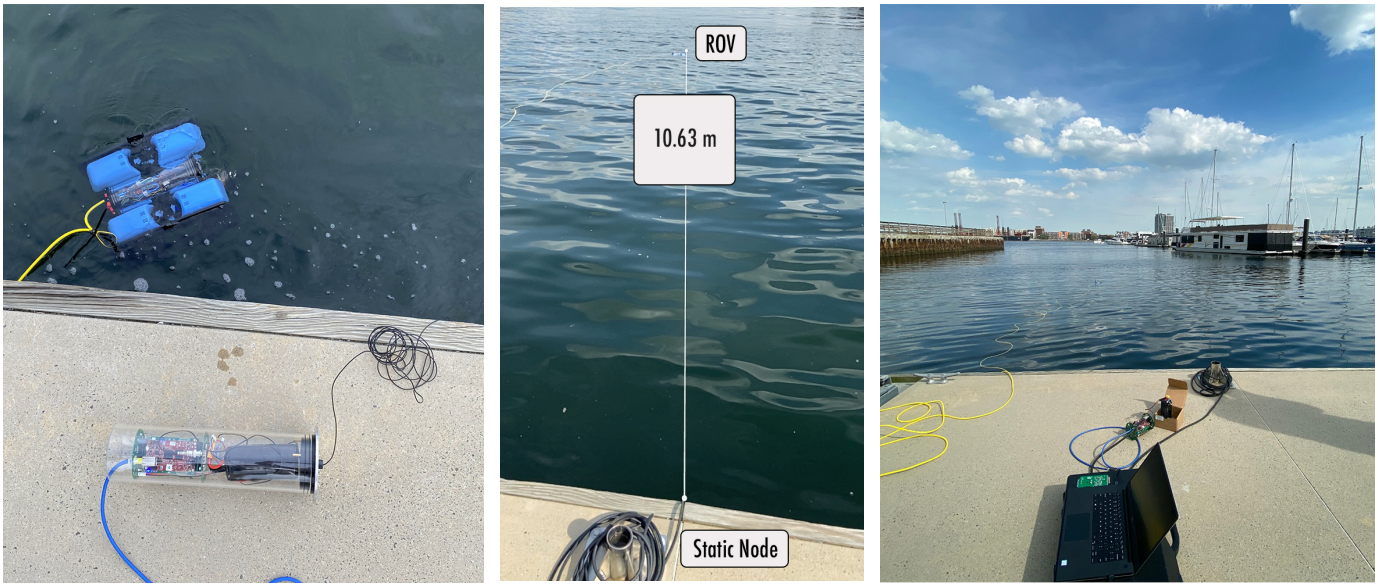

(a) (b) (c)

Fig. 3: Different views of the deployment scenario. (a) A modem integrated to the UV (mobile node) and a single modem with a fixed location (static node); (b) Initial node placement: The static and mobile nodes are placed 10.63 m apart; (c) The experiment location.

then be estimated with

$$v = a \times c \tag{2}$$

where c is the speed of sound.

TABLE I: ZP-OFDM Physical Layer parameter sets for high and medium throughput packets.

Parameter	High Throughput	Medium Throughput
Bandwidth	62.5 kHz	125 kHz
Modulation	QPSK	BPSK
# of Symbols	16	1
Data subcarr.	2816	5632
Pilot subcarr.	1024	2048
Null subcarr.	256	512
Guard Int.	25 ms	25 ms
Data Rate	54.7 kbit/s	19.2 kbit/s

System bandwidth and carrier frequency are determined during the deployment with preliminary measurement and characterization. To that end, two nodes are deployed at the side of the dock. They used the Medium Throughput packets (see Table I) which incorporate equally spaced pilot and null subcarrier at a center frequency of 125 kHz for characterization. Figure 4 shows subcarrier SNR measurements. The results indicate almost a 30 dB difference in SNR between 70 kHz and 130 kHz which is attributed to transmitting voltage response of the B-Tech transducer. To avoid using these low SNR regions of the frequency spectrum, the High Throughput packet structure (see Table I) at a 125 kHz center frequency is chosen for this set of experiments.

In the experiments, two different deployment scenarios are considered, namely, stationary and mobile. The stationary scenario is used to characterize the system for the link performance while the mobile scenario is to investigate the effect of mobility.

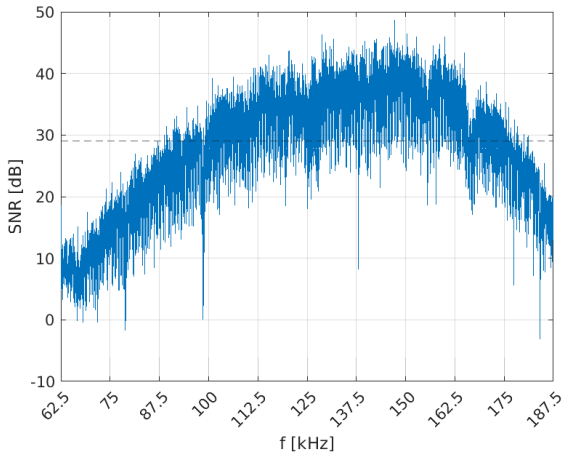

Fig. 4: Subcarrier SNR measurement with 125 kHz bandwidth ZP-OFDM packets.

In the stationary scenario, the mobile node is positioned at approximately 10 m and the static modem is at the middle of the side of the dock as illustrated in 3b. The static node transducer is submerged 1.2 m below the waterline. The ROV is set to depth hold mode at 1 m as the transducer position is roughly 20 cm below the depth sensor of the ROV. For this scenario, high throughput data is transmitted continuously while the transmit power level setting on the mobile node is

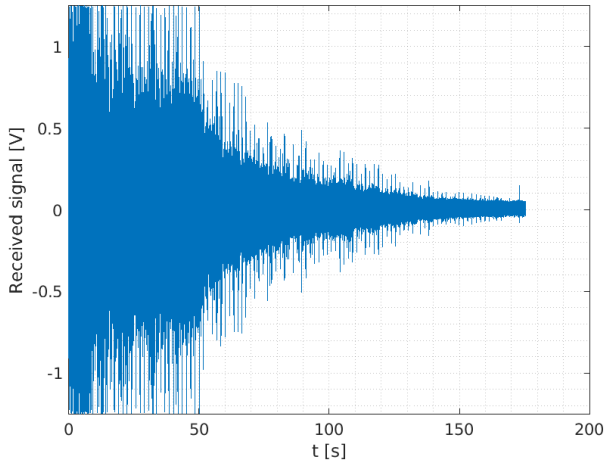

Fig. 5: Received signal amplitude in the stationary scenario.

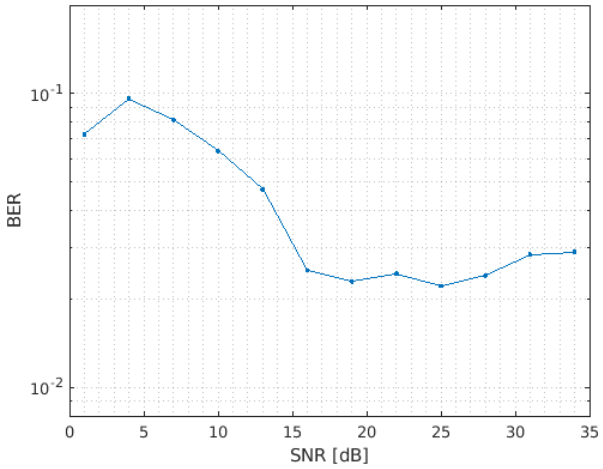

Fig. 6: BER vs. SNR in stationary scenario for QPSK modulated ZP-OFDM packets with $62.5\,\mathrm{kHz}$ bandwidth.

varied in $3\,\mathrm{dB}$ decrements from full power ($0\,\mathrm{dB}$) down to $-36\,\mathrm{dB}$. The variation of the power level is made possible by a variable gain control block inside the PL which is modified from the host computer through the modem configuration software. The static node is designated as the receiver due to differences in their transducers as explained previously. The orientation of the mobile node is important because of the directivity of its transducer and it needs to face the direction of the static node during communication. The ROV, on the other hand, experiences forces in different directions due to currents which both drift and rotate the mobile node. To counter link distance reduction and orientation perturbation, the operator performed correcting maneuvers during the recordings.

In the mobile scenario, the initial position is the same as the stationary scenario with $10\,\mathrm{m}$ link distance. The operator moves the mobile node towards the static node using a controller. For these recordings, the ROV is operated at half gain since we have found that slower movement makes it difficult to identify Doppler shifts while the ROV drifts with currents. On the other hand, higher speed movement causes deviation from trajectory due to drag forces on the payload section of the mobile node. As the link distance decreases with the movement, channel attenuation diminishes which may result in a high received signal level. To prevent such distortion transmit level is set for $20\,\mathrm{dB}$ attenuation for this scenario.

The received signal level in the stationary scenario is shown in Fig. 5, where variation of the transmit power level over time can be observed clearly. The corresponding bit error rate (BER) and signal-to-noise ratio (SNR) measured at the receiver are given in Fig. 6. BER drops below 3×10^{-2} above $15\,\mathrm{dB}$ SNR. However, as the SNR gets larger, the BER curve flattens out and does not improve. In this case, while the individual subcarrier SNR is measured to be increasing, the received signal is also at the limits of the input range as seen in Fig. 5. This implies that the signal is distorted at the receiver preamplifier circuit and clipped at the input of the ADC. The preamplifier circuit is designed with the highest possible sensitivity to increase the range of operation but in this case, the received signal is too high even when the variable gain amplifier gain is off.

The received signal level for the the mobile deployment scenario, can be observed in in Fig. 7. The received signal level is increasing between $20 - 35\,\mathrm{s}$ as the channel attenuation decreases. Fig. 8 shows the SNR calculated from the received packet. The SNR curve is correlated to the received signal but fluctuations can be observed at times. Moreover, the SNR loss due to transducer directivity can be observed after $40\,\mathrm{s}$ as the operator rotates the ROV in the yaw axis to prevent crashing into the dock. Similarly, a few more points can be identified (i.e. around $22\,\mathrm{s}$) in which maneuvers are performed by the operator to preserve ROVs orientation.

The estimated speed of the mobile node is shown in Fig. 9. The node starts moving at $19\,\mathrm{s}$ and stops at $34.2\,\mathrm{s}$. During the trajectory, the average speed is estimated to be 0.63 m/s from

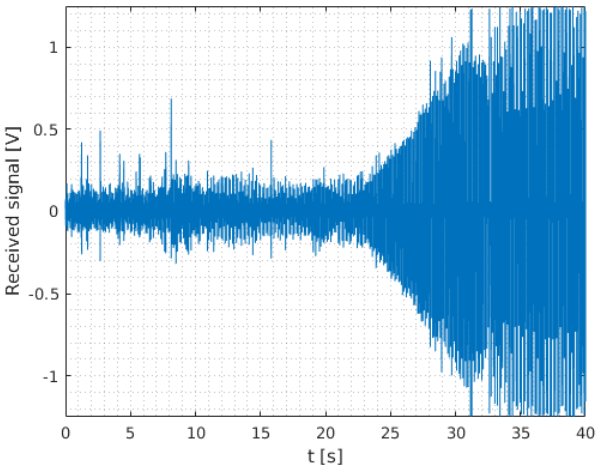

Fig. 7: Received signal level in the mobile scenario.

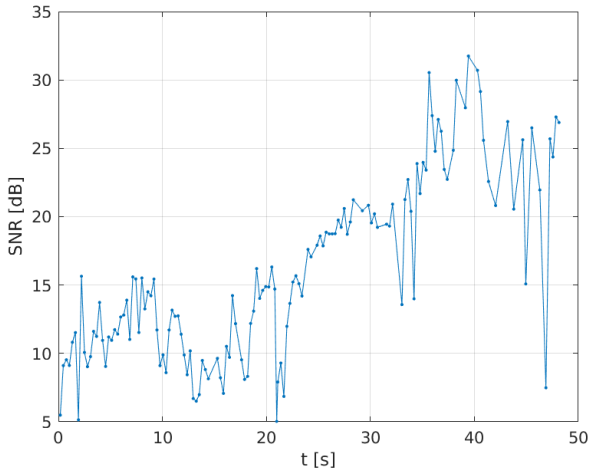

Fig. 8: Signal-to-Noise-Ratio (SNR) in the mobile scenario.

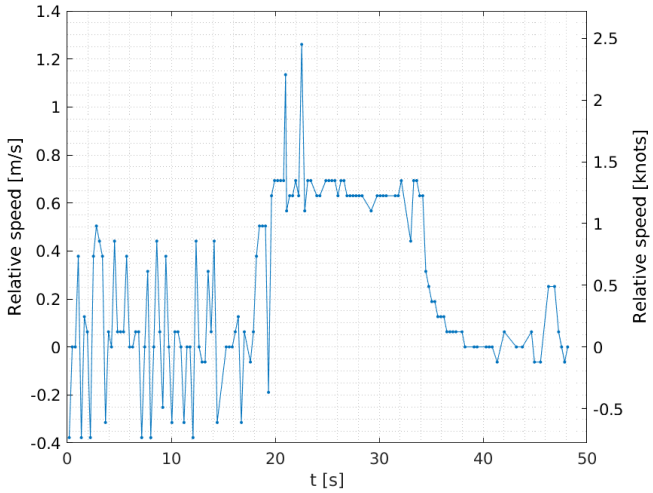

Fig. 9: Estimated speed in the mobile scenario.

Doppler scaling factors. Note that this corresponds to $52.5\,\mathrm{Hz}$ frequency shift at the center frequency of the system. The shift is significantly larger than the subcarrier bandwidth used in ZP-OFDM packets. The time duration between endpoints was measured as $15.2\,\mathrm{s}$ and from estimated speed, the distance of the trajectory is approximated as $9.6\,\mathrm{m}$. This estimate is reasonable considering the uncertainty of the measurement of the initial position and the trajectory ends at a distance to the side of the dock.

IV. Conclusions

This paper presents the design blueprint of a wireless UV that integrates a custom software-defined underwater acoustic networking modem with a commercially available underwater vehicle (UV). The paper provides key software, hardware, and mechanical design principles as well as a detailed system description. Finally, the paper presents a set of sea experiments, where the proposed system is utilized to generate a sample dataset with link performances are characterized with different physical layer parameters under varying mobility and channel conditions.

Acknowledgments

This work was supported in part by the National Science Foundation grants CNS-1763964 and CNS-1726512.

References

[1] T. Melodia, H. Kulhandjian, L. Kuo, and E. Demirors, "Advances in Underwater Acoustic Networking," in *Mobile Ad Hoc Networking: Cutting Edge Directions*, second edition ed., S. Basagni, M. Conti, S. Giordano, and I. Stojmenovic, Eds. Inc., Hoboken, NJ: John Wiley and Sons, 2013, pp. 804–852.

[2] Forbes, "Drones begin to deliver on their potential for the oil and gas sector," 2018, https://tinyurl.com/s8yo6ka9.

[3] D. Khojasteh and R. Kamali, "Design and dynamic study of a ROV with application to oil and gas industries of Persian Gulf," *Ocean Engineering*, vol. 136, pp. 18–30, 2017.

[4] CNBC, "Underwater drones join hunt for trillions in mineral riches trapped on ocean's floor," 2020, https://tinyurl.com/7ndxhre.

[5] R. A. Armstrong, H. Singh, J. Torres, R. S. Nemeth, A. Can, C. Roman, R. Eustice, L. Riggs, and G. Garcia-Moliner, "Characterizing the deep insular shelf coral reef habitat of the Hind Bank marine conservation district (US Virgin Islands) using the Seabed autonomous underwater vehicle," *Continental Shelf Research*, vol. 26, no. 2, pp. 194–205, 2006.

[6] ITNews, "Swarms of tiny robots could help Defence clear underwater mines," 2020, https://tinyurl.com/39hvshzl.

[7] "FMC ROV Systems," 2020. [Online]. Available: https://www.technipfmc.com/en/what-we-do/subsea/Robotics/rov-systems

[8] F. A. Azis, M. S. M. Aras, M. Z. A. Rashid, M. N. Othman, and S. S. Abdullah, "Problem identification for underwater remotely operated vehicle (ROV): A case study," *Procedia Engineering*, vol. 41, pp. 554–560, 2012.

[9] R. B. Wynn, V. A. I. Huvenne, T. P. Le Bas, B. J. Murton, D. P. Connelly, B. J. Bett, H. A. Ruhl, K. J. Morris, J. Peakall, D. R. Parsons, E. J. Sumner, S. E. Darby, R. M. Dorrell, and J. E. Hunt, "Autonomous underwater vehicles (AUVs): Their past, present and future contributions to the advancement of marine geoscience," *Marine Geology*, vol. 352, pp. 451–468, 2014.

[10] "WaterLinked," 2021. [Online]. Available: https://www.waterlinked.com/

[11] E. Demirors, J. Shi, A. Duong, N. Dave, R. Guida, B. Herrera, F. Pop, G. Chen, C. Cassella, S. Tadayon, M. Rinaldi, S. Basagni, M. Stojanovic, and T. Melodia, "The SEANet project: Toward a programmable internet of underwater things," in *Proceedings of UComms 2018*, Lerici, Italy, August 28–30 2018, pp. 1–5.

[12] M. Stojanovic and J. Preisig, "Underwater acoustic communication channels: Propagation models and statistical characterization," *IEEE Communications Magazine*, vol. 47, no. 1, pp. 84–89, January 2009.

[13] B. Li, S. Zhou, M. Stojanovic, L. Freitag, and P. Willett, "Multicarrier communication over underwater acoustic channels with nonuniform doppler shifts," *IEEE Journal of Oceanic Engineering*, vol. 33, no. 2, pp. 198–209, April 2008.